URSI GASS 2020, Rome, Italy, 29 August - 5 September 2020

Dyadic Green's Function Studies for the Three-shell Head Model

Grigorios P. Zouros[(1)], Georgios D. Kolezas[(1)], George Fikioris[(1)], and Nikolaos L. Tsitsas*[(2)]
(1) School of Electrical and Computer Engineering, National Technical University of Athens, 15780 Athens, Greece
(2) School of Informatics, Aristotle University of Thessaloniki, 54124 Thessaloniki, Greece

Abstract

In this work, we employ analytical expressions for the calculation of the dyadic Green's function (DGF) of the isotropic three-shell head model, due to an infinitesimal electric dipole located in the internal core that corresponds to the brain. We compute the electric field obtained from this DGF and compare and validate our analytical results with HFSS commercial software when the dipole is inside a single sphere. Then, we numerically examine the behavior of the electric field due to the placement of the dipole inside a three-shell spherical head model. Finally, we discuss how the isotropic model can be extended to the more complicated anisotropic one by considering a volume integral equation approach.

1 Introduction

The accurate computation of the interaction of electromagnetic waves with biological tissues has direct biomedical applications in modern deep brain stimulation (DBS) treatment, with the latter being used to treat Parkinson's disease [1], depression [2], or in applications like pacemakers [3]. DBS is achieved through surgical implants of electrodes, which act as electrical sources and render local parts of the brain inactive for treatment needs. The measurement of the electric or magnetic activity of this internal source interaction is carried out through electroencephalography (EEG) or magnetoencephalography (MEG). In biological imaging, EEG or MEG is performed via multilayered spherical models, where, in each layer, the conductivity changes significantly. The most realistic head model routinely adopted is the three-layered one, consisting of the brain (the core in the three-layered configuration), the skull and the scalp (the outer layer) [4], while other, more complicated models exist, in which conductivity is considered anisotropic [5].

The use of finite element and finite difference methods revealed that the errors obtained from the spherical shape are of the same order of magnitude with those obtained due to the inaccurate knowledge of the electrical properties of the head [6]. Numerical methods, however, face high computational load due to the large discretization they require, otherwise they cannot accurately approximate the multilayered and anisotropic properties of the head, especially when the stimulation is within the region of inhomogeneity (i.e., inside the brain) [7]. This is because, for accurate computations, a minimum number of samples per wavelength is required in each individual layer. For multilayered structures, this results in a high number of finite elements, and as a consequence, in high memory consumption and time-consuming execution of the algorithm. Therefore, what is commonly adopted in practice, is to reduce the discretization to obtain a low computational time, but with an impact on reduced accuracy.

In this work, we focus our study on the three-shell model [4], and extract analytical formulas for expressing the DGF due to an infinitesimal electric dipole located in the internal core, which corresponds to the brain [8]. In particular, the DGF of the multilayered configuration is decomposed in two terms: a singular term that corresponds to the DGF with constitutive parameters of the respective isotropic layer, and a regular dyadic term to be computed. We present and discuss numerical results on the electric field generated by the dipole when the latter is placed inside the core-brain of the three-shell model. To establish validity, the electric field obtained from the analytical solution is compared with HFSS, first for the simplified single sphere, and second for the three-layered sphere.

2 DGF Formulation for the Head Model

We consider a spherical human head model consisting of three concentric spheres, each having radius $r = a_p$ $(p = 1,2,3)$, with $a_3 < a_2 < a_1$. The spheres divide the head into three homogeneous layers, namely, V_3 $(0 \leq r < a_3)$, V_2 $(a_3 < r < a_2)$, and V_1 $(a_2 < r < a_1)$. Each layer V_p has permittivity ε_p and permeability μ_p. The surrounding medium is free space, which is assumed as an unbounded outer layer V_0 $(r > a_1)$, with permittivity ε_0 and permeability μ_0. The configuration is excited by an infinitesimal electric dipole with dipole moment $\mathbf{p}$, located in layer V_3. A time dependence of the form $\exp(-\mathbf{i}\omega t)$ is assumed and suppressed throughout.

The electric field induced in layer V_p by the electric dipole located at $\mathbf{r} = \mathbf{r}_s$ in layer V_3 is given by [8]

$$\mathbf{E}^p(\mathbf{r};\mathbf{r}_s) = \mathbf{i}\omega\mu_p\tilde{\mathbf{G}}^p(\mathbf{r};\mathbf{r}_s)\cdot\mathbf{p}, \quad \mathbf{r} \in V_p, \tag{1}$$

where $\tilde{\mathbf{G}}^p$ is the component of the configuration's DGF in layer V_p. For layers V_p $(p = 0,1,2)$, $\tilde{\mathbf{G}}^p$ can be expressed

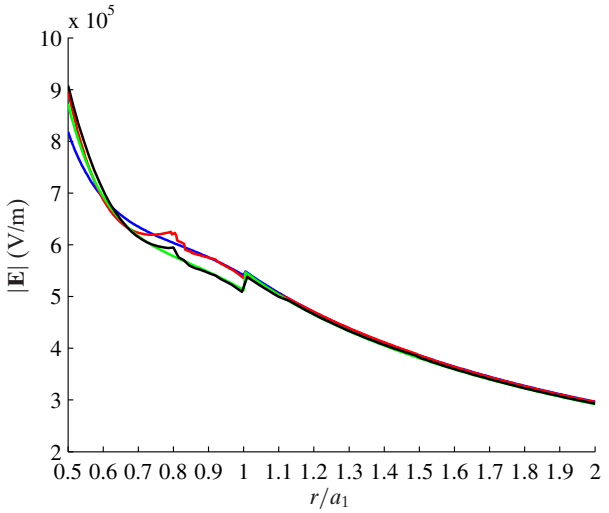

Figure 1. Magnitude of total electric field **E** on x-axis for a single sphere, when the dipole is z-oriented. Values of parameters: $k_0 a_1 = 0.6\pi$, $\varepsilon_{r1} = 2.54$, $\mu_{r1} = 1$. Blue and red curves: dipole location on z-axis at $r/a_1 = r_s/a_1 = 0.1$; blue: analytical solution; red: HFSS. Green and black curves: dipole location on z-axis at $r/a_1 = r_s/a_1 = 0.2$; green: analytical solution; black: HFSS.

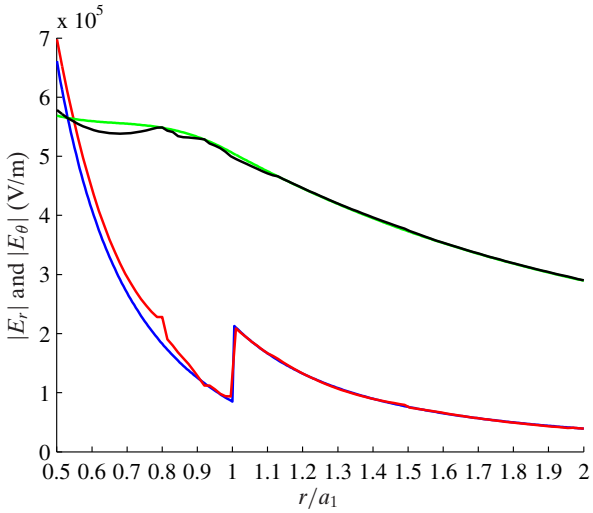

Figure 2. Magnitude of electric field components E_r and E_θ on x-axis for the same configuration with the one in Fig. 1. Dipole's location is on z-axis at $r/a_1 = r_s/a_1 = 0.2$. Blue and red curves: $|E_r|$; blue: analytical solution; red: HFSS. Green and black curves: $|E_\theta|$; green: analytical solution; black: HFSS.

as a series of spherical vector wave functions as

$$\begin{aligned}\tilde{\mathbf{G}}^p(\mathbf{r};\mathbf{r}') = {} & \frac{ik_3}{4\pi}\sum_{n=1}^{\infty}\sum_{m=0}^{n}\sum_{\sigma=e,o}\frac{2n+1}{n(n+1)}\varepsilon_m\frac{(n-m)!}{(n+m)!}\times \\ & \Big\{\mathbf{M}^{(1)}_{\sigma mn}(k_p,\mathbf{r})\Big[\alpha_n^p\mathbf{M}^{(1)}_{\sigma mn}(k_3,\mathbf{r}')+\beta_n^p\mathbf{M}^{(3)}_{\sigma mn}(k_3,\mathbf{r}')\Big] \\ & +\mathbf{N}^{(1)}_{\sigma mn}(k_p,\mathbf{r})\Big[\gamma_n^p\mathbf{N}^{(1)}_{\sigma mn}(k_3,\mathbf{r}')+\delta_n^p\mathbf{N}^{(3)}_{\sigma mn}(k_3,\mathbf{r}')\Big] \\ & +\mathbf{M}^{(3)}_{\sigma mn}(k_p,\mathbf{r})\Big[\tilde{\alpha}_n^p\mathbf{M}^{(1)}_{\sigma mn}(k_3,\mathbf{r}')+\tilde{\beta}_n^p\mathbf{M}^{(3)}_{\sigma mn}(k_3,\mathbf{r}')\Big] \\ & +\mathbf{N}^{(3)}_{\sigma mn}(k_p,\mathbf{r})\Big[\tilde{\gamma}_n^p\mathbf{N}^{(1)}_{\sigma mn}(k_3,\mathbf{r}')+\tilde{\delta}_n^p\mathbf{N}^{(3)}_{\sigma mn}(k_3,\mathbf{r}')\Big]\Big\}. \quad (2)\end{aligned}$$

In (2), $\mathbf{M}^{(j)}_{\sigma mn}$ and $\mathbf{N}^{(j)}_{\sigma mn}$, are the even/odd spherical vector wave functions of the first ($j=1$) and third ($j=3$) kind [9], $k_p = \omega\sqrt{\varepsilon_p\mu_p}$, $k_3 = \omega\sqrt{\varepsilon_3\mu_3}$, and $\varepsilon_m = 1$ for $m = 0$, while $\varepsilon_m = 2$ for $m \neq 0$.

In the case of layer V_3 which contains the dipole source, the DGF component is given by

$$\tilde{\mathbf{G}}^3(\mathbf{r};\mathbf{r}') = \tilde{\mathbf{G}}^{\rm pr}(\mathbf{r};\mathbf{r}') + \tilde{\mathbf{G}}^{\rm sec}(\mathbf{r};\mathbf{r}'). \quad (3)$$

In (3), $\tilde{\mathbf{G}}^{\rm pr}$ is the primary contribution that corresponds to the DGF of the unbounded medium filled with the material of layer V_3, and has the expression [8]

$$\begin{aligned}\tilde{\mathbf{G}}^{\rm pr}(\mathbf{r};\mathbf{r}') = {} & \\ & -\frac{\hat{\mathbf{r}}\hat{\mathbf{r}}}{k_3^2}\delta(\mathbf{r}-\mathbf{r}')+\frac{ik_3}{4\pi}\sum_{n=1}^{\infty}\sum_{m=0}^{n}\sum_{\sigma=e,o}\frac{2n+1}{n(n+1)}\varepsilon_m\frac{(n-m)!}{(n+m)!}\times \\ & \left\{\begin{bmatrix}\mathbf{M}^{(3)}_{\sigma mn}(k_3,\mathbf{r})\mathbf{M}^{(1)}_{\sigma mn}(k_3,\mathbf{r}')+\mathbf{N}^{(3)}_{\sigma mn}(k_3,\mathbf{r})\mathbf{N}^{(1)}_{\sigma mn}(k_3,\mathbf{r}')\\ \mathbf{M}^{(1)}_{\sigma mn}(k_3,\mathbf{r})\mathbf{M}^{(3)}_{\sigma mn}(k_3,\mathbf{r}')+\mathbf{N}^{(1)}_{\sigma mn}(k_3,\mathbf{r})\mathbf{N}^{(3)}_{\sigma mn}(k_3,\mathbf{r}')\end{bmatrix}\right., \quad (4)\end{aligned}$$

where the upper branch is taken if $r > r'$ and the lower one if $r < r'$, while δ denotes the Dirac delta function. The secondary contribution $\tilde{\mathbf{G}}^{\rm sec}$ corresponds to the scattering by the boundaries of the spherical shells, and is expanded as in the right-hand side of (2) with $p = 3$.

The expansion coefficients α_n^p, β_n^p, γ_n^p, δ_n^p, $\tilde{\alpha}_n^p$, $\tilde{\beta}_n^p$, $\tilde{\gamma}_n^p$, and $\tilde{\delta}_n^p$ in (2), are determined by employing a recursive algorithm, as described in detail in [8]. In this way, we obtain an analytical expression for the DGF of the head model, which can be used for field calculations, as we demonstrate in the following Section.

3 Numerical Results

Herein, we examine the behavior of the electric field generated due to an infinitesimal electric dipole located inside the three-shell spherical configuration. To do so, we first compute the DGF in each layer by (2) and then the respective electric field from (1). We first consider a single sphere with normalized electric size $k_0 a_1 = 0.6\pi$, where k_0 is the free space wavenumber. The sphere's relative permittivity is set at $\varepsilon_{r1} = 2.54$, while its relative permeability is equal to unity. Fig. 1 depicts the magnitude $|\mathbf{E}| = \sqrt{|E_r|^2+|E_\theta|^2+|E_\varphi|^2}$ of the total electric field when the dipole is z-oriented and located at two different points on z-axis, i.e., at $r/a_1 = r_s/a_1 = 0.1$ and at $r/a_1 = r_s/a_1 = 0.2$. The observation path for $|\mathbf{E}|$ is along x-axis and specifically starts above the actual location of the source, i.e., at $r/a_1 = 0.5$, and ends up one radius of additional length outside the sphere, i.e., at $r/a_1 = 2$. The reason for not depicting results below $r/a_1 = 0.5$ is that in HFSS, in order to set-up the dipole configuration, one should define a surrounding sphere that encloses the dipole. The field mag-

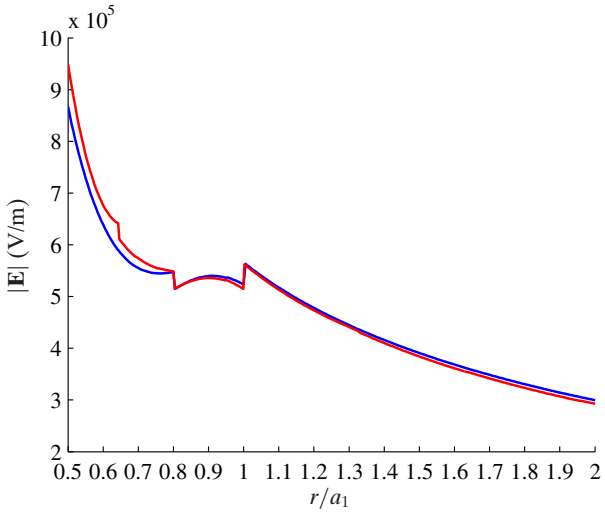

Figure 3. Magnitude of total electric field **E** on x-axis for a three-shell sphere, when the dipole is z-oriented and located at $r/a_1 = r_s/a_1 = 0.2$. Values of parameters: $k_0 a_1 = 0.6\pi$, $a_2/a_1 = 0.95$, $a_3/a_1 = 0.8$, $\varepsilon_{r1} = 4$, $\varepsilon_{r2} = 5$, $\varepsilon_{r3} = 2.54$, $\mu_{r1} = \mu_{r2} = \mu_{r3} = 1$. Blue curve: analytical solution; red curve: HFSS.

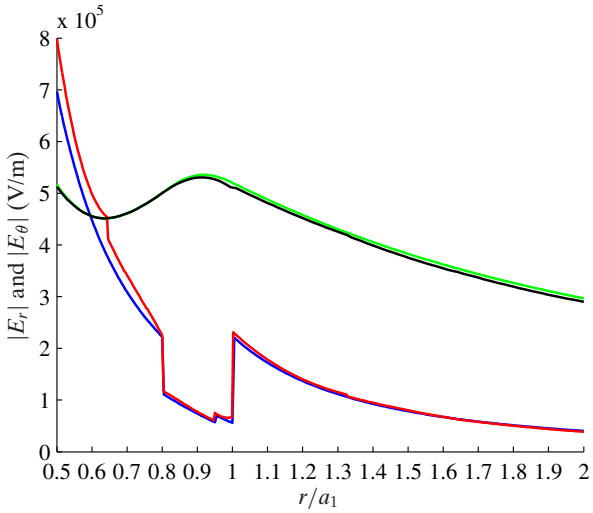

Figure 4. Magnitude of electric field components E_r and E_θ on x-axis for the same configuration with the one in Fig. 3. Blue and red curves: $|E_r|$; blue: analytical solution; red: HFSS. Green and black curves: $|E_\theta|$; green: analytical solution; black: HFSS.

nitude inside this sphere is artificial and equals the field on the surface of that sphere. Therefore, in order to compare the analytical solution with HFSS and establish validity, we should compare results outside this surrounding sphere. From Fig. 1 we observe the very good agreement between the analytical solution and HFSS, for both dipole's locations, while the discontinuity at the surface $r/a_1 = 1$ is evident due to the change of the material parameters.

In Fig. 2 we plot the electric field components E_r and E_θ for the same configuration as in Fig. 1 and for the same observation path, but when the dipole is located at $r/a_1 = r_s/a_1 = 0.2$. Obviously the agreement with HFSS is evident. Since $|E_\theta|$ is tangential to the spherical surface, it is continuous as it crosses the $r/a_1 = 1$ point, while $|E_r|$ clearly depicts a step discontinuity. The $|E_\varphi|$ component is from one up to two orders of magnitude smaller than $|E_r|$, $|E_\theta|$, thus negligible, and for that reason is not depicted.

Having established the validity for the single sphere, we now proceed to the three-shell model. The values of the parameters used are gathered in the caption of Fig. 3, with the latter depicting results for $|\mathbf{E}|$ for the same observation points as in Fig. 1. Now, due to the change of layers at $r/a_1 = a_3/a_1 = 0.8$ and at $r/a_1 = a_2/a_1 = 0.95$, there are two discontinuities at these points, in addition to the one at the outer interface at $r/a_1 = 1$. It should be noted that the discontinuity at $r/a_1 = 0.95$ is not clearly depicted in Fig. 3 and one should zoom in to distinguish it. Again, the comparison with HFSS clearly shows the validity of the analytical solution.

Finally, to complement the study for the three-layered sphere, in Fig. 4 we present plots for the magnitude of E_r and E_θ components. Now, all three discontinuities of the E_r are clearly observed, while E_θ is continuous as it passes through all layers. These properties are well captured by both the analytical solution and HFSS, thus verifying the validity of the proposed analytical method.

4 Conclusion and Future Work

We have computed and examined the behavior of the electric field in a three-shell spherical head model, excited by an infinitesimal electric dipole located in the core of the configuration. This task has been carried out by first computing the DGF in each layer. The proposed analytical solution has been validated versus HFSS, showing a very good agreement.

Extensions of the present work consist the use of more than three layers to model the head, and the improvement of the simplified model presented here to the more complicated anisotropic one [5]. Obviously, this latter task is quite challenging. A workaround may be the consideration of a volume integral equation method for the evaluation of the unknown DGF, while the anisotropic multilayers will be handled by integration in a similar manner as in the electromagnetic scattering by anisotropic spheres [10].

5 Acknowledgements

This research is co-financed by Greece and the European Union (European Social Fund-ESF) through the Operational Programme "Human Resources Development, Education and Lifelong Learning 2014–2020" in the context of the project "Deep brain stimulation modeling through accurate electrodynamic techniques" (MIS 5047942).

References

[1] S. Little, A. Pogosyan, S. Neal, B. Zavala, L. Zrinzo, M. Hariz, T. Foltynie, P. Limousin, K. Ashkan, J. FitzGerald, A. L. Green, T. Z. Aziz, and P. Brown, "Adaptive deep brain stimulation in advanced Parkinson disease," *Annals of Neurology*, vol. 74, pp. 449–457, 2013.

[2] T. E. Schlaepfer, B. H. Bewernick, S. Kayser, B. Mädler, and V. A. Coenen, "Rapid effects of deep brain stimulation for treatment-resistant major depression," *Biological Psychiatry*, vol. 73, pp. 1204–1212, 2013.

[3] J. Kruse and C. Redmond, "Detecting and distinguishing cardiac pacing artifacts," *Analog Dialogue*, vol. 46, pp. 13–18, 2012.

[4] M. Stenroos, A. Hunold, and J. Haueisen, "Comparison of three-shell and simplified volume conductor models in magnetoencephalography," *NeuroImage*, vol. 94, pp. 337–348, 2014.

[5] T. Miinalainen, A. Rezaei, D. Us, A. Nüßing, C. Engwer, C. H. Wolters, and S. Pursiainen, "A realistic, accurate and fast source modeling approach for the EEG forward problem," *NeuroImage*, vol. 184, pp. 56–67, 2019.

[6] E. C. Morales, C. D. Acosta-Medina, G. Castellanos-Dominguez, and D. Mantini, "A finite-difference solution for the EEG forward problem in inhomogeneous anisotropic media," *Brain Topography*, vol. 32, pp. 229–239, 2019.

[7] E. Bilgin and A. Yapar, "Electromagnetic scattering by radially inhomogeneous dielectric spheres," *IEEE Trans. Antennas Propag.*, vol. 63, pp. 2677–2685, 2015.

[8] P. Prokopiou and N. L. Tsitsas, "Electromagnetic excitation of a spherical medium by an arbitrary dipole and related inverse problems," *Studies Appl. Math.*, vol. 140, pp. 438–464, 2018.

[9] J. A. Stratton, *Electromagnetic Theory*. New York: McGraw-Hill, 1941.

[10] G. P. Zouros and G. C. Kokkorakis, "Electromagnetic scattering by an inhomogeneous gyroelectric sphere using volume integral equation and orthogonal Dini-type basis functions," *IEEE Trans. Antennas Propag.*, vol. 63, pp. 2665–2676, 2015.